

An efficient solver for volumetric scattering based on fast spherical harmonics transforms

Youngae Han

Lorentz Solution, Inc.

October 29, 2018

Abstract

The Helmholtz equation arises in the study of electromagnetic radiation, optics, acoustics, etc. In spherical coordinates, its general solution can be written as a spherical harmonic series which satisfies the radiation condition at infinity, ensuring that the wave is outgoing. The boundary condition at infinity is hard to enforce with a finite element method since a suitable approximation needs to be made within reasonable distance from scatterers. Luckily, the Helmholtz equation can be represented as a Lippmann-Schwinger integral equation which removes the necessity of the boundary approximations and its Green's function can be expanded as a spherical harmonic series which leads to our numerical scheme based on spherical harmonic polynomial transform. In this paper, we present an efficient solver for the Helmholtz equation which costs $O(N \log N)$ operations, where N is the number of the discretization points. We use the fast spherical harmonic transforms which are originally developed in [33]. The convergence order of the method is tied to the global regularity of the solution. At the lower end, it is second order accurate for discontinuous material properties. The order increases with increasing regularity leading to spectral convergence for globally smooth solutions.

Keywords: Helmholtz equation, fast spherical harmonic transform, addition theorem, Lippmann-Schwinger integral equation, radiation condition, wave equation, Spectral convergence.

1 Introduction

Computational electromagnetics and acoustics are fundamental to understanding of many practical systems like scattering, microwave circuits, radar, antennas, remote sensing, seismic exploration, ultrasound and tomography. Therefore, the demand for efficient numerical simulations of electromagnetic and acoustic fields is only increasing. The electromagnetic field is the solution of Maxwell's equations which are coupled with more than one unknown. These equations can be uncoupled by raising their order resulting in the wave equation. Thus, the Helmholtz equation reduced from the wave equation has been a classical problem ([5],

[23]) to solve and central focus of research for many decades and still drawing ongoing attentions. Using the separation of variables, the Helmholtz equation has been analytically solved for a simple geometry with homogeneous medium. In particular, for a spherical geometry, the solution is analytically given as the spherical harmonic series expansion in the angular direction and Bessel series expansion along the radial direction ([5]) which inspires our numerical method based on spherical harmonic series expansion that is particularly efficient for spherical objects. There have been many efforts to develop fast polynomial transformations ([12], [15], [22], [19], [33]) to have equivalent speed advantages like FFTs. Here, we used the fast spherical harmonic transforms ([19]) developed in [33] which is based on fast multipole method ([15]) to have $O(N \log N)$ costs comparable to those based on FFTs while enjoying that the separation of variables that results from the addition theorem ([10]). This readily translates into quadratures that converge with higher order than those implicit in FFT-based schemes.

For the Helmholtz equation concerned in this paper is to find the scattered field generated due to the incident field with outgoing radiation condition. The most popular numerical methods are finite element methods (FEM) ([13], [18], [21], [26], [34]) and integral equation methods (IEM) ([1], [7], [8], [19], [20], [29], [35]). Although FEM can handle arbitrarily shaped obstacles with ease and the resulting matrix is sparse, it imposes a serious difficulty in solving scattering problems arising from the infinite size of domain. For this reason, great effort has gone into the design of approximate local boundary conditions and perfectly matched layers ([2], [3], [17]) that minimize spurious reflections which is by no means a trivial matter ([18]). Integral equation methods (IEM), on the other hand, implicitly account for radiation conditions through the use of *outgoing* Green's functions. This very use of singular Green's functions, on the other hand, also translates into numerical challenges. Moreover, these methods lead to a linear system involving a full matrix and thus they are not competitive unless a specialized strategy is used to accelerate matrix-vector products; examples of accelerated IEM include those based on FFTs ([7], [20], [28]) and those that use fast multipole expansions ([16], [25], [27]).

In this paper, inspired by the work in ([6], [7], [20]), we present a new accelerated IEM based on the addition theorem ([10]) and fast spherical harmonic transforms ([19], [33]). The convergence rate of our new algorithms is tied to the global regularity of fields. In particular, they converge with second order for the most singular case of discontinuous material properties and with increased rates for more regular arrangements; for smooth configurations the convergence is spectral. This paper is organized as follows. The Lippmann-Schwinger integral equation is presented in Section 2. The numerical factorization of the integral equation based on spherical harmonic series expansion is explained in Section 3. In Section 4, numerical implementations and their expected costs are derived, and in Section 5, numerical examples are given to confirm the predicted performance of the algorithms described in Section 4. Finally, in Section 6, the content of this paper is summarized.

2 Lippmann-Schwinger integral equation

The wave equation states that

$$\frac{\partial^2 u}{\partial t^2} = \frac{c_0^2}{n^2} \nabla^2 u \quad (1)$$

where $n(r)$ is the refractive index and c_0 is the propagation speed of the wave in air. If we assume that the wave function is time-harmonic as

$$u(r, t) = u(r)e^{-i\omega t},$$

then a spatial solution $u(r)$ satisfies the Helmholtz equation

$$\Delta u + k^2 n^2 u = 0 \text{ in } \mathbb{R}^3. \quad (2)$$

Here we will consider the scattering problem to determine the total field generated by a given incident field u^i . Then the total field u which is the sum of u^i and the scattered field u^s satisfies equation (2) while u^i is the solution of

$$\Delta u^i + k^2 u^i = 0 \text{ in } \mathbb{R}^3. \quad (3)$$

The *Sommerfeld radiation condition* is given at infinity which guarantees that the scattered field is outgoing,

$$\lim_{r \rightarrow \infty} r \left(\frac{\partial u^s}{\partial r} - iku^s \right) = 0. \quad (4)$$

This boundary condition must be approximated at the reasonable distance from scatterers which is the main challenge to solve the Helmholtz equation. But, this problem can be avoided if one appeals to the equivalent *Lippmann-Schwinger integral equation* which states

$$u(x) = u^i(x) - k^2 \int_{\Omega} \Phi(x, y) u(y) m(y) dy, \quad x \in \mathbb{R}^3 \quad (5)$$

where $m = 1 - n(x)^2$ and the inhomogeneity is of compact support Ω . Therefore, we will develop an efficient solver based on the Lippmann-Schwinger integral equation.

3 Spherical harmonic series expansion

To solve the integral equation (5), we resort to the spherical harmonic series expansions of the Green's function $\Phi(x, y)$. The addition theorem in [10] states that

$$\begin{aligned} \Phi(x, y) &= \frac{1}{4\pi} \frac{e^{ik|x-y|}}{|x-y|} \\ &= ik \sum_{n=0}^{\infty} \sum_{m=-n}^n h_n^{(1)}(k\rho_{>}) Y_n^m(\hat{\rho}_{>}) j_n(k\rho_{<}) \overline{Y_n^m(\hat{\rho}_{<})} \end{aligned} \quad (6)$$

where

$$\begin{aligned} x &= \tilde{\rho}(\sin \tilde{\theta} \cos \tilde{\varphi}, \sin \tilde{\theta} \sin \tilde{\varphi}, \cos \tilde{\theta}), \\ y &= \rho(\sin \theta \cos \varphi, \sin \theta \sin \varphi, \cos \theta), \\ \rho_{<} &= \min(\rho, \tilde{\rho}) \text{ and } \rho_{>} = \max(\rho, \tilde{\rho}). \end{aligned}$$

So, if we approximate u and u^i by a truncated spherical harmonic series as

$$u^F(\rho, \theta, \phi) = \sum_{n=0}^F \sum_{m=-n}^n u_n^m(\rho) Y_n^m(\theta, \phi) \quad (7)$$

$$u^{i,F}(\rho, \theta, \phi) = \sum_{n=0}^F \sum_{m=-n}^n u_n^{i,m}(\rho) Y_n^m(\theta, \phi) \quad (8)$$

then from equation (5) and the orthogonality properties of the spherical harmonics, $m(r)$ can be approximated without losing accuracy as

$$m^{2F}(\rho, \theta, \phi) = \sum_{n=0}^{2F} \sum_{m=-n}^n m_n^m(\rho) Y_n^m(\theta, \phi). \quad (9)$$

Therefore, the formulation in (5) becomes

$$u_n^m(\rho) = u_n^{i,m}(\rho) + iK_n^m(\rho), \quad (10)$$

where

$$K_n^m(\rho) = -k^3 \int_0^{\mathbf{R}} h_n^{(1)}(k\rho_{>}) j_n(k\rho_{<}) I_n^m(\rho) \rho^2 d\rho, \quad (11)$$

and

$$I_n^m(\rho) = \int_{\phi=0}^{2\pi} \int_{\theta=0}^{\pi} u^F(\rho, \theta, \phi) m^{2F}(\rho, \theta, \phi) \overline{Y_n^m(\theta, \phi)} \sin \theta d\theta d\phi, \quad (12)$$

$n = 0, 1, \dots, F$. To solve the formulation in (10), we use the linear solver GMRES which requires the fast evaluation of angular integration of $I_n^m(\rho)$ in (12) and the radial evaluation of $K_n^m(\rho)$ in (11).

4 Numerical implementation

4.1 Angular integration

Due to the orthogonality of spherical harmonics, equation (12) can be written as

$$u^F(\rho, \theta, \phi) m^{2F}(\rho, \theta, \phi) = \sum_{n=0}^{3F} \sum_{m=-n}^n I_n^m(\rho) Y_n^m(\theta, \phi). \quad (13)$$

Therefore, we define spherical harmonic transform as

$$\{f(\theta_i, \phi_j)\}_{i,j=0}^{2F+1} \rightarrow \{\{c_n^m\}_{m=-n}^n\}_{n=0}^F \quad (14)$$

where

$$f(\theta_i, \phi_j) = \sum_{n=0}^F \sum_{m=-n}^n c_n^m Y_n^m(\theta_i, \phi_j)$$

and its inverse, for appropriate choices of the angles $\{\theta_i, \phi_j\}$; see [33], [19].

In [33], it is shown that if we define S_n^m as

$$Y_n^m(t, \phi) = S_n^{|m|}(t) e^{im\phi}$$

then

$$\sum_{n=0}^{N-1} c_n^m S_{m+n}^m(x_j^N), \quad j \in \{0, 1, 2, \dots, N-1\} \quad (15)$$

can be computed in $O(N \log N)$ operations for arbitrary x_j^N .

This work leads to fast spherical harmonic transform (FSHT) and its inverse (IFSHT) and these polynomial transforms cost $O(F^2 \log F)$ for (14). Thus, $I_n^m(\rho)$ of (12) is computed as follows

$$\begin{aligned} \{\{I_n^m(\rho)\}_{m=-n}^n\}_{n=0}^F &= FSHT_{3F}(IFSHT_{3F}(\{\{u_n^m(\rho)\}_{m=-n}^n\}_{n=0}^F) \\ &\cdot IFSHT_{3F}(\{\{m_n^m(\rho)\}_{m=-n}^n\}_{n=0}^{2F})). \end{aligned} \quad (16)$$

Therefore, the angular integration costs $O(F^2 \log F)$ for each ρ .

4.2 Radial integration

The radial integral $K_n^m(\rho)$ in (11) has a corner-type singularity at $\rho = \tilde{\rho}$ therefore, we write it as

$$\begin{aligned} \frac{-K_n^m(a)}{k^3} &= h_n^{(1)}(ka) \int_0^{\min(a, \mathbf{R})} j_n(k\rho) I_n^m(\rho) \rho^2 d\rho + j_n(ka) \int_{\min(a, \mathbf{R})}^{\mathbf{R}} h_n^{(1)}(k\rho) I_n^m(\rho) \rho^2 d\rho \\ &= i \left[y_n(ka) \int_0^{\min(a, \mathbf{R})} j_n(k\rho) I_n^m(\rho) \rho^2 d\rho + j_n(ka) \int_{\min(a, \mathbf{R})}^{\mathbf{R}} y_n(k\rho) I_n^m(\rho) \rho^2 d\rho \right] \\ &\quad + j_n(ka) \int_0^{\mathbf{R}} j_n(k\rho) I_n^m(\rho) \rho^2 d\rho. \end{aligned} \quad (17)$$

Although it is numerically challenging to evaluate the Hankel function $h_n^{(1)}(k\rho)$, the product of the $j_n(k\rho)$ and $h_n^{(1)}(k\rho)$ is bounded which leads us to define modified Bessel functions

$\tilde{j}_n(\rho)$ and $\tilde{y}_n(\rho)$ in the form

$$\begin{aligned}\tilde{j}_n(\rho) &:= \frac{1 \cdot 3 \cdot 5 \cdots (2n+1)}{\rho^n} j_n(\rho) = \left[1 - \frac{\frac{1}{2}\rho^2}{1!(2n+3)} + \frac{(\frac{1}{2}\rho^2)^2}{2!(2n+3)(2n+5)} + \cdots \right] \\ \tilde{y}_n(\rho) &:= \frac{\rho^{n+1}}{-1 \cdot 1 \cdot 3 \cdot 5 \cdots (2n-1)} y_n(\rho) = \left[1 - \frac{\frac{1}{2}\rho^2}{1!(1-2n)} + \frac{(\frac{1}{2}\rho^2)^2}{2!(1-2n)(3-2n)} + \cdots \right]\end{aligned}\tag{18}$$

and with these modified Bessel functions we obtain

$$\begin{aligned}K_n^m(a) &= \frac{i}{2n+1} \left[\tilde{y}_n(ka) \int_0^{\min(a, \mathbf{R})} \left(\frac{\rho}{a}\right)^{n+1} \tilde{j}_n(k\rho) I_n^m(\rho) k^2 \rho d\rho \right. \\ &\quad \left. + \tilde{j}_n(ka) \int_{\min(a, \mathbf{R})}^{\mathbf{R}} \left(\frac{a}{\rho}\right)^n \tilde{y}_n(k\rho) I_n^m(\rho) k^2 \rho d\rho \right] \\ &\quad + \tilde{j}_n(ka) (ka)^n \int_0^{\mathbf{R}} \frac{(k\rho)^n (-2n-1) k^3}{1 \cdot 3^2 \cdot 5^2 \cdots (2n+1)^3} \tilde{j}_n(k\rho) I_n^m(\rho) \rho^2 d\rho.\end{aligned}\tag{19}$$

For the radial integration, we divide the integration domain in a number N_i of equi-length interpolation intervals $U_j = [u_j^0, u_j^1]$, $1 \leq j \leq N_i$ on which we approximate for $\rho \in U_j$,

$$I_n^m(\rho) \approx \sum_{l=0}^{N_d-1} c_{l,m,n}^j T_l^{u_j^0, u_j^1}(\rho),\tag{20}$$

where

$$T_l^{u_j^0, u_j^1}(\rho) = T_l\left(\frac{\rho - (u_j^1 + u_j^0)/2}{(u_j^1 - u_j^0)/2}\right)$$

are the Chebyshev polynomials in U_j . It costs $O(N_d(\log N_d)N_i)$ to compute the Chebyshev coefficients of $I_n^m(\rho)$ for fixed n and m . If we denote $\{\rho_k^j\}_{k=1}^{N_d}$ the Chebyshev points in U_j , the following equation holds

$$\begin{aligned}\int_0^{\rho_{k+1}^j} \rho^{n+2} \tilde{j}_n(k\rho) I_n^m(\rho) d\rho &= \int_0^{\rho_k^j} \rho^{n+2} \tilde{j}_n(k\rho) I_n^m(\rho) d\rho \\ &\quad + \sum_{l=0}^{N_d-1} c_{l,m,n}^j \int_{\rho_k^j}^{\rho_{k+1}^j} \rho^{n+2} \tilde{j}_n(k\rho) T_l^{u_j^0, u_j^1}(\rho) d\rho.\end{aligned}\tag{21}$$

Therefore, if the moments $\int_{\rho_k^j}^{\rho_{k+1}^j} \rho^{n+2} \tilde{j}_n(k\rho) T_l^{u_j^0, u_j^1}(\rho)$ are computed and stored, then it costs

$O(N_d^2 N_i)$ to compute $\int_0^{\rho_k^j} \rho^{n+2} \tilde{j}_n(k\rho) I_n^m(\rho) d\rho$ for $1 \leq j \leq N_i$ and $1 \leq k \leq N_d$. Similarly, the

computation of $\int_{\rho_k^j}^{\mathbf{R}} \rho^{1-n} \tilde{y}_n(k\rho) I_n^m(\rho) d\rho$ also costs $O(N_d^2 N_i)$ for $1 \leq j \leq N_i$ and $1 \leq k \leq N_d$.

With these moments and precomputed coefficients $C_1(a)$, $C_2(a)$ and $C_3(a)$, $K_n^m(a)$ can be written as

$$\begin{aligned} K_n^m(a) &= C_1(a) \int_0^{\min(a, \mathbf{R})} \rho^{n+2} \tilde{j}_n(k\rho) I_n^m(\rho) d\rho \\ &+ C_2(a) \int_{\min(a, \mathbf{R})}^{\mathbf{R}} \rho^{1-n} \tilde{y}_n(k\rho) I_n^m(\rho) d\rho \\ &+ C_3(a) \int_0^{\mathbf{R}} \rho^{n+2} \tilde{j}_n(k\rho) I_n^m(\rho) d\rho. \end{aligned} \quad (22)$$

Therefore the total cost for radial integration is

$$O[N_i N_d F^2 (\log N_d + N_d + 1)] = O(N).$$

5 Numerical examples

To show the predicted performance of the algorithm, four examples are presented below.

Example 5.1 Consider the scattering off a homogeneous sphere of radius 1 and the refractive index $n(x) = 2$. In this case, the problem is explicitly solvable, therefore comparison with the exact solution is possible. A plane wave incident in the positive z -direction can be written as

$$e^{ik\vec{x} \cdot (0,0,1)} = e^{ik\rho \cos\theta} = \sum_{n=0}^{\infty} i^n (2n+1) j_n(k\rho) P_n(\cos\theta). \quad (23)$$

If we differentiate equation (23) m_{inc} times with respect to $t = \cos\theta$, we obtain the incident wave extended from (23) as

$$\begin{aligned} u^i &= \rho^{|m_{inc}|} e^{ik\rho \cos\theta} \sin^{|m_{inc}|} \theta e^{im_{inc}\phi} \\ &= \sum_{n=|m_{inc}|}^{\infty} \frac{i^n (2n+1)}{(ik)^{|m_{inc}|}} j_n(k\rho) \frac{\sqrt{4\pi(n+|m_{inc}|)!}}{\sqrt{(2n+1)(n-|m_{inc}|)!}} Y_n^{m_{inc}}(\theta, \phi). \end{aligned} \quad (24)$$

For this incidence the exact solution [5] is

$$u^s = \begin{cases} \sum_{n=|m_{inc}|}^{\infty} \{a_n j_n(2k\rho) - Q_n^{|m_{inc}|}(k, \rho)\} Y_n^{m_{inc}}(\theta, \phi), & \rho \leq 1 \\ \sum_{n=|m_{inc}|}^{\infty} b_n h_n(k\rho) Y_n^{m_{inc}}(\theta, \phi), & \rho \geq 1 \end{cases}$$

where

$$Q_n^{|m_{inc}|}(k, \rho) = \frac{i^n (2n+1)}{(ik)^{|m_{inc}|}} j_n(k\rho) \frac{\sqrt{4\pi(n+|m_{inc}|)!}}{\sqrt{(2n+1)(n-|m_{inc}|)!}}.$$

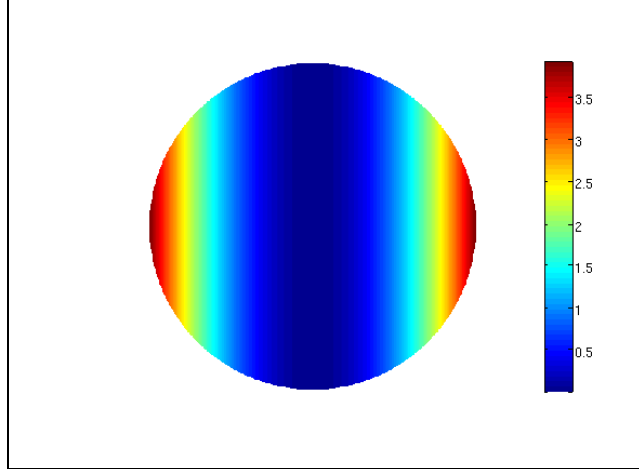


Figure 1: The incident field intensity $|u^i|^2$ where $m_{inc} = 1$ for examples 5.1-5.3.

By enforcing C^1 continuity of u^s along the material discontinuity, $\{a_n\}$ and $\{b_n\}$ are determined. The numerical error is computed as $E = \|u_{exact} - u_{approx}\|_\infty$ between the approximate and exact solutions for $m_{inc} = 1$ and $k = 5$ in (24) and different values of the interpolation orders N_d in (20) in Tables 1-3.

N_i	time per iteration	GMRES iteration	relative error	error ratio
2^3	54 (sec)	34	0.564482	
2^4	108 (sec)	35	0.20477	2.81207
2^5	217 (sec)	36	0.0532706	3.7178

Table 1: Radial convergence for Example 5.1: the sphere centered at the origin.
Parameters: $m_{inc} = 1$, $k = 5$, $F = 2^5 - 1$, $N_d = 2$, $0 \leq \rho \leq 2$,
GMRES tolerance = $1e - 10$.

N_i	time per iteration	GMRES iteration	relative error	error ratio
2^3	108 (sec)	35	0.00192818	
2^4	217 (sec)	36	0.000193606	10.0197
2^5	435 (sec)	36	1.35701e-05	14.1395

Table 2: Radial convergence for Example 5.1 for $N_d = 4$, GMRES tolerance = $1e - 10$,
Same parameters as in table 1.

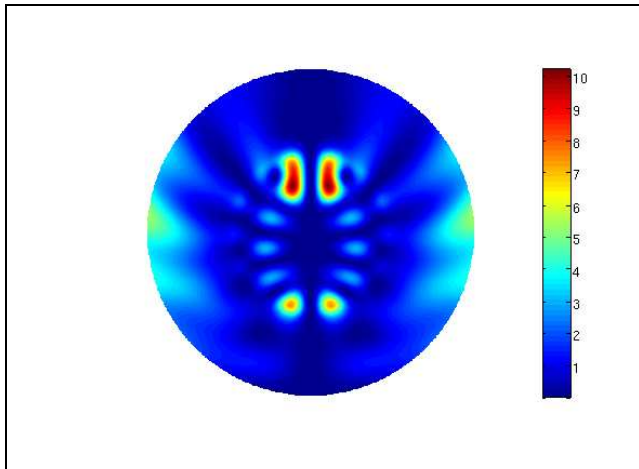


Figure 2: The field intensity $|u|^2$ for example 5.1 where $m_{inc} = 1$, $k = 5$.

N_i	time per iteration	GMRES iteration	relative error	error ratio
2^3	218 (sec)	69	2.92336e-08	
2^4	435 (sec)	67	1.70495e-10	171.523
2^5	1098 (sec)	66	6.61144e-13	257.404

Table 3: Radial convergence for Example 5.1 for $N_d = 8$, GMRES tolerance = $1e - 15$, Same parameters as in table 1.

Example 5.2 To test the convergence when there is a material discontinuity for the angular integration, we consider the same sphere as in example 5.1 but now centered at $(0, 0, d)$. For this case, we can obtain the incident wave as

$$\begin{aligned}
 u^i &= (x^2 + y^2)^{\frac{|m_{inc}|}{2}} e^{ik(z-d)} e^{im_{inc}\phi} \\
 &= e^{-ikd} \sum_{n=|m_{inc}|}^{\infty} Q_n^{|m_{inc}|}(k, \rho) Y_n^{m_{inc}}(\theta)
 \end{aligned} \tag{25}$$

and the exact spherical harmonic series expansion for $m(x)$ as follows

$$\begin{aligned}
 m(\rho, \theta) &= (1 - n_0^2) \left(\sum_{n=1}^{\infty} \frac{2n+1}{2} \sqrt{(1 - \cos^2 \theta_0)} \frac{(n-1)!}{(n+1)!} P_n^1(\cos \theta_0) \sqrt{\frac{4\pi}{2n+1}} Y_n^0(\theta, \phi) \right. \\
 &\quad \left. + \frac{1}{2} (1 - \cos \theta_0) \sqrt{4\pi} Y_0^0(\theta, \phi) \right)
 \end{aligned}$$

where $0 \leq (d-r) \leq \rho \leq (d+r)$, $n_0 = 2$ is the refractive index and $(\rho \sin \theta_0, \rho \cos \theta_0)$ is a solution of

$$y^2 + z^2 = \rho^2, \quad y^2 + (z-d)^2 = r^2.$$

The exact solution is obtained from the spherical harmonic transform of the exact values computed from the solution in example 5.1 with shifting. In tables 4-6 we present radial and angular convergence studies for this case where the discontinuity does not lie on the grid.

N_i	time per iteration	GMRES iteration	relative error	error ratio
2^5	1203 (sec)	26	0.299451	
2^6	2408 (sec)	27	0.0817522	3.64575
2^7	4987 (sec)	27	0.020442	3.99036

Table 4: Radial convergence for Example 5.2: the sphere centered at (0,0,2) with radius 1. Parameters: $m_{inc} = 1$, $k = 5$, $F = 2^7 - 1$, $N_d = 2$, $0 \leq \rho \leq 4$, GMRES tolerance = $1e - 5$.

N_i	time per iteration	GMRES iteration	relative error	error ratio
2^4	601 (sec)	6	2.88611e-05	
2^5	1203 (sec)	6	8.11132e-06	3.51951
2^6	2406 (sec)	6	1.97643e-06	4.0819

Table 5: Radial convergence for Example 5.2: the sphere centered at (0,0,2) with radius 1. Parameters: $m_{inc} = 3$, $k = 1$, $F = 2^7 - 1$, $N_d = 2$, $0 \leq \rho \leq 4$, GMRES tolerance = $1e - 10$.

F	time per iteration	GMRES iteration	relative error	error ratio
2^4-1	352 (sec)	21	1.9425	
2^5-1	866 (sec)	26	0.113651	17.0918
2^6-1	2061 (sec)	27	0.00157294	72.2536

Table 6: Angular convergence for Example 5.2: the sphere centered at (0,0,2) with radius 1. Parameters: $m_{inc} = 1$, $k = 5$, $N_d = 2$, $N_i = 2^7$, $0 \leq \rho \leq 4$, GMRES tolerance = $1e - 5$.

Example 5.3 To test the convergence of a non-spherical object, we consider a square rotated by 45 degree and axisymmetric along z direction. The refractive index $n(r)$ is 2 in $|x+y| \leq 1$ shown in Figure 3. The incident wave is the same as in example 5.1. We present radial and angular convergence studies in tables 7-9.

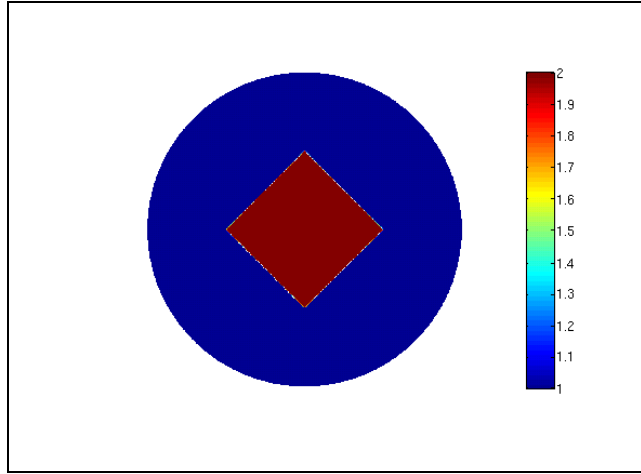


Figure 3: The scatterer for example 5.3.

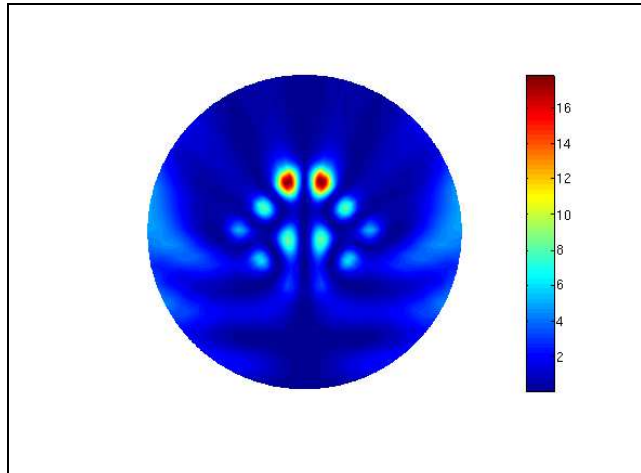


Figure 4: The field intensity $|u|^2$ for example 5.3 where $m_{inc} = 1$, $k = 5$.

N_i	time per iteration	GMRES iteration	relative error	error ratio
2^4	259 (sec)	20	0.606676	
2^5	559 (sec)	20	0.0568001	10.6809
2^6	1081 (sec)	20	0.0416413	1.36403
2^7	2072 (sec)	20	0.0126427	3.29371

Table 7: Radial convergence for Example 5.3: the square rotated by 45 degree.

Parameters: $m_{inc} = 1$, $k = 5$, $F = 2^6 - 1$, $N_d = 2$, $0 \leq \rho \leq 2$,
GMRES tolerance = $1e - 5$.

N_i	time per iteration	GMRES iteration	relative error	error ratio
2^7	2072 (sec)	8	0.000389159	
2^8	4135 (sec)	8	0.000123866	3.14176
2^9	8729 (sec)	8	1.79324e-05	6.90739
2^{10}	17823 (sec)	8	3.94232e-06	4.54869

Table 8: Radial convergence for Example 5.3: the square rotated by 45 degree.

Parameters: $m_{inc} = 1$, $k = 1$, $F = 2^6 - 1$, $N_d = 2$, $0 \leq \rho \leq 2$,
GMRES tolerance = $1e - 10$.

F	time per iteration	GMRES iteration	relative error	error ratio
2^4-1	177 (sec)	26	0.0328253	
2^5-1	436 (sec)	26	0.00439355	7.47126
2^6-1	1036 (sec)	26	0.000548512	8.00994

Table 9: Angular convergence for Example 5.3: the square rotated by 45 degree.

Parameters: $m_{inc} = 1$, $k = 5$, $N_d = 2$, $N_i = 2^6$, $0 \leq \rho \leq 2$,
GMRES tolerance = $1e - 10$.

Example 5.4 The final example is to show the dependence of the scheme on the regularity of the scattering medium. We consider a refractive index given by

$$n(\rho, \cos \theta) = \begin{cases} (1 + |\cos \theta|^\beta \sin^{|m_{ref}|} \theta e^{im_{ref}\phi})^{1/2}, & 1 \leq \rho \leq 2 \\ 1, & 0 \leq \rho < 2 \text{ or } \rho > 2. \end{cases} \quad (26)$$

Then,

$$m(\rho, t) = \begin{cases} -|t|^\beta (1 - t^2)^{\frac{|m_{ref}|}{2}} e^{im_{ref}\phi}, & 1 \leq \rho \leq 2 \\ 0, & 0 \leq \rho < 1 \text{ or } \rho > 2 \end{cases}$$

and the exact spherical harmonic series expansion for $m(\rho, t)$ is given by $\sum_{l=0}^{\infty} m_{2l}(\rho) Y_{|m_{ref}|+2l}^{m_{ref}}(t)$, where

$$\begin{aligned}
m_{2l}(\rho) &= - \int_{\phi=0}^{2\pi} \int_{\theta=0}^{\pi} Y_{|m_{ref}|+2l}^{m_{ref}}(\theta, \phi) \cos^{\beta} \theta \sin^{|m_{ref}|} \theta e^{im_{ref}\phi} \cos \theta d\theta d\phi \\
&= - \sqrt{\frac{(2n+1)(n-|m_{ref}|)!}{(n+|m_{ref}|)!}} \frac{\pi}{2^{\beta+|m_{ref}|}} \frac{\Gamma(1+\beta)}{\Gamma(1+\frac{\beta}{2})} \frac{1}{\Gamma(\frac{3}{2}+\frac{\beta}{2})} \\
&\quad \cdot \frac{\prod_{s=0}^{l-1} (\frac{1}{2}\beta - s)}{\prod_{s=0}^{|m_{ref}|+l-1} (\frac{1}{2}\beta + \frac{3}{2} + s)} \frac{(n+|m_{ref}|)!}{(n-|m_{ref}|)!}.
\end{aligned} \tag{27}$$

In tables 10-12, we present the order of convergence for $\beta = 0.4, 1.4, 2.4$ to show the correlation between smoothness of the refractive index $n(x)$ and the order of convergence.

F	time per iteration	GMRES iteration	relative error	log₂(error ratio)
2 ³ -1	83 (sec)	6	0.00186872	
2 ⁴ -1	419 (sec)	6	7.42083e-06	7.97625
2 ⁵ -1	2048 (sec)	6	1.19402e-06	2.63575

Table 10: Angular convergence for Example 5.4 for $\beta = 0.4$ ($m \in C^{0.4}$, $u \in C^{2.4}$).
Parameters: $m_{inc} = 3$, $m_{ref} = 1$, $k = 0.5$, $N_d = 8$, $N_i = 4$, $0 \leq \rho \leq 4$,
GMRES tolerance = $1e - 10$.

F	GMRES iteration	relative error	log₂(error ratio)
2 ³ -1	5	0.0018687	
2 ⁴ -1	5	6.99546e-07	11.3833
2 ⁵ -1	5	5.82286e-08	3.58662

Table 11: Angular convergence for Example 5.4 for $\beta = 1.4$ ($m \in C^{1.4}$, $u \in C^{3.4}$).
Same parameters as in table 10.

F	GMRES iteration	relative error	log₂(error ratio)
2 ³ -1	5	0.00186869	
2 ⁴ -1	5	6.6957e-08	14.7684
2 ⁵ -1	5	2.74242e-09	4.60971

Table 12: Angular convergence for Example 5.4 for $\beta = 2.4$ ($m \in C^{2.4}$, $u \in C^{4.4}$).
Same parameters as in table 10.

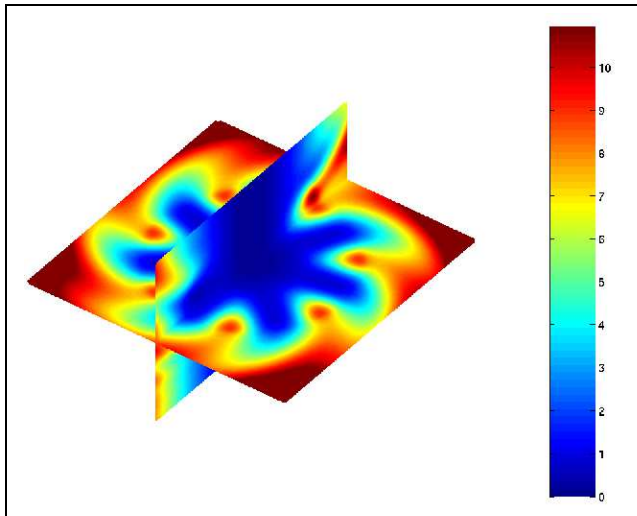


Figure 5: The field intensity $|u|^2$ for example 5.4 where $m_{inc} = 1$, $m_{ref} = 7$, $\beta = 0.2$, $k = 5$.

6 Summary

In this paper, an efficient solver for scattering by penetrable three-dimensional structures is presented. The solution is obtained by the iterative evaluation of Lippmann-Schwinger integral equation and its efficiency comes from the use of the addition theorem and fast spherical harmonics transforms. The scheme allows for such evaluations in $O(N \log N)$ operations, where N is the number of the discretization points. The convergence order of the method, on the other hand, is tied to the global regularity of the solution. At the lower end, it is second order accurate for discontinuous material properties. The order increases with increasing regularity of the refractive index leading to spectral convergence for globally smooth solutions.

Acknowledgments

Y. Han would like to thank Dr. E. M. Hyde for a helpful discussion. This work was in part supported by AFOSR Contract F49620-02-1-0052.

References

- [1] A. Anand and F. Reitich, *An efficient high-order algorithm for acoustic scattering from penetrable thin structures in three dimensions*, *J. Acoust. Soc. Amer.* *121* (2007), 2503-2514.
- [2] J.-P. Berenger, *A perfectly matched layer for the absorption of electromagnetic waves*, *J. Comput. Phys.* *114* (2) (1994) 185-200.

- [3] J.-P. Berenger, *Three-dimensional perfectly matched layer for the absorption of electromagnetic waves*, *J. Comput. Phys.* 127 (1996) 363-379.
- [4] S. Belmehdi, *On the associated Legendre polynomials*, *J. Comput. Appl. Math.*, 32(1990), pp. 311-319.
- [5] C. A. Balanis, *Advanced engineering electromagnetics*, John Wiley and Sons, Inc., 1989.
- [6] O. P. Bruno and A. Sei, *A fast high-order solver for EM scattering from complex penetrable bodies: TE case*, *IEEE Trans. Antennas. Propagat.*, Vol. 42, pp. 859-862, June 1994.
- [7] O. P. Bruno and E. M. Hyde, *High-order fourier approximation in scattering by two-dimensional, inhomogeneous media*, *SIAM J. Numer. Anal.* Vol. 42, No. 6, pp. 2298-2319, 2005.
- [8] O. P. Bruno and L. A. Kunyansky, *A fast, high-order algorithm for the solution of surface scattering problems: basic implementation, tests and applications*, in *Journal of Computat. Physics*, vol. 169, pp. 80-110, May 2001.
- [9] O. P. Bruno, Y. Han and M. M. Pohlman, *Accurate, high-order representation of complex three-dimensional surfaces via Fourier continuation analysis*, in *Journal of Computat. Physics*, vol. 227, pp. 1094-1125, Dec 2007.
- [10] D. Colton and R. Kress, *Inverse acoustic and electromagnetic scattering theory*, second edition, Springer-Verlag, Heidelberg New York, 1998.
- [11] T. S. Chihara, *An Introduction to orthogonal polynomials*, Gordon and Breach, New York 1978.
- [12] J. R. Driscoll, D. M. Healy, jr. and D. N. Rockmore, *Fast discrete polynomial transforms with applications to data analysis for distance transitive graphs*. *Siam J. Comput.*, Vol. 26, No. 4, pp. 1066-1099, Aug. 1997.
- [13] C. I. Goldstein, *A Finite Element Method for Solving Helmholtz Type Equations in Waveguides and Other Unbounded Domains*, in *Math. of Computat.*, Vol. 39, No. 160, pp. 309-324, Oct. 1982.
- [14] L. Greengard, *The rapid evaluation of potential fields in particle systems*, MIT press, 1988.
- [15] L. Greengard and V. Rokhlin, *A fast algorithm for particle simulations*, *J. Comp. Phys.*, Vol. 73, 1987, pp. 325-348.
- [16] L. Greengard, J. Huang, V. Rokhlin, W. Stephen, *Accelerating fast multipole methods for the Helmholtz equation at low frequencies*, *IEEE Comput. Sci. Engrg.* 5 (3) (1998) 3238.

- [17] T. Ha and I. Kim, *Analysis of one-dimensional Helmholtz equation with PML boundary*, *J. Comput. Phys.* 206 (1) (2007) 586-598.
- [18] I. Harari, *A survey of finite element methods for time-harmonic acoustics*, *Comput. Methods Appl. Mech. Engrg.* 195 (2006), pp. 1594-1607.
- [19] Y. Han, *Efficient high-order volumetric scattering solvers based on fast polynomial transforms*, *University of Minnesota, Phd thesis*, 2004.
- [20] E. M. Hyde and O. P. Bruno, *A fast, high-order solver for scattering by penetrable bodies of three dimensions*, in *Journal of Computat. Physics*, vol. 202, pp. 236-261, Jan. 2005.
- [21] F. Ihlenburg and I. Babuska, *Finite Element Solution of the Helmholtz Equation with High Wave Number Part II: The h-p Version of the FEM*, *SIAM J. Numer. Anal.* Vol. 34 (1), pp. 315-358, 1997.
- [22] M. A. Inda, R. H. Bisseling and D. K. Maslen, *On the efficient parallel computation of Legendre transforms*. *Siam J. Sci. Comput.*, Vol. 23, No. 1, pp. 271-303, 2001.
- [23] J. D. Jackson, *Classical Electrodynamics*, *John Wiley and Sons, Inc.*, 1962.
- [24] R. Kress, *Linear integral equations*, *Springer-Verlag, Heidelberg New York* 1989.
- [25] F. Ling, J. M. Jin, and J. M. Song, *Multilevel Fast Multipole Algorithm for Analysis of Large-Scale Microstrip Structures*, *Micro. Opt. Tech. Lett.*, 9, pp. 508-510, 1999.
- [26] Ya Yan Lu, *A fourth-order Magnus scheme for Helmholtz equation*, *J. Comput. Phys.* 173 (2) (2005) 247-258.
- [27] Y. C. Pan, W. C. Chew, and L. X. Wan, *A Fast Multipole Method Based Calculation of the Capacitance Matrix for Multiple Conductors above Stratified Dielectric Media*, *IEEE Trans. Microwave Theory Tech.*, vol 49, pp. 480-490, 2001.
- [28] J. R. Phillips and J. K. White, *Efficient Capacitance Computation of 3D Structures Using Generalized Pre-Corrected FFT Methods*, in *Proceedings of the 3rd Topical Meeting on Electric Performance of Electronic Packaging*, Monterey, 1994, California.
- [29] V. Rokhlin, *Rapid Solution of Integral Equations of Scattering Theory in Two Dimensions*, *J. Comput. Phys.*, 36, 2, pp. 414-439, 1990.
- [30] A. E. Ruehli, *Equivalent Circuit Models for Three-Dimensional Multiconductor Systems*, in *IEEE Trans. Microwave theory and tech.*, vol. MTT-22, No. 3, March 1974.
- [31] T. J. Rivlin, *Chebyshev polynomials*, *New York, Wiley*, 1974.
- [32] Sansone, *Orthogonal functions*, *Interscience publishers, inc.*, *New York*, pp. 208-216, 1959.

- [33] R. Suda and M. Takami, *A fast spherical harmonics transform algorithm*, *Math. Comp.* 71 (2002), pp. 703-715.
- [34] L. L. Thompson and P. M. Pinsky, *A Galerkin Least Squares Finite Element Method for the Two-Dimensional Helmholtz Equation*, *Internat. J. for Numer. Methods in Engineering* Vol.38, pp. 371-397 (1995).
- [35] J. Zhao, *Electromagnetic Simulator Systems*, in *Patent No. US 7,562,000 B2*, Jul. 14, 2009.